ADVANCES IN MATERIALS SCIENCE, Vol. 23, No. 1 (75), March 2023

DOI: 10.2478/adms-2023-0003

Maroua Layachi [1], Abdelhak Khechai*[2], Abderrahmane Ghrieb[1], Safa Layachi[2]

[1]*Laboratory of Development in Mechanics and Materials, University of Djelfa, Djelfa, Algeria*
[2]*Laboratoire de Recherche en Génie Civil, LRGC, Université de Biskra, Biskra, Algeria*

**a.khechai@univ-biskra.dz*

NUMERICAL FAILURE ANALYSIS OF LAMINATED BEAMS USING A REFINED FINITE ELEMENT MODEL

ABSTRACT

In the present investigation, laminated composite beams subjected to a bending static loading are studied in order to determine their failure mechanisms and the first ply failure (FPF) load. The FPF analysis is performed using a refined rectangular plate element. The present element is formulated based on the classical lamination theory (CLT) to calculate the in-plane stresses. To achieve this goal, several failure criterions, including Tsai-Wu, Tsai-Hill, Hashin, and Maximum Stress criteria, are used to predict failure mechanisms. These criterions are implemented within the finite element code to predict the different failure damages and responses of laminated beams from the initial loading to the final failure. The numerical results obtained using the present element compare favorably with those given by the analytic approaches. It is observed that the numerical results are very close to the analytical results, which demonstrates the accuracy of the present element. Finally, several parameters, such as fiber orientations, stacking sequences, and boundary conditions, are considered to determine and understand their effects on the strength of these laminated beams.

Keywords*: composite materials; beam; bending; failure; finite element*

INTRODUCTION

High-performance composite materials were used in order to manufacture aircrafts, marine vehicles, and various structures. Due to their features such as high specific strength, stiffness, and lightweight, the application of these composite materials has now gone beyond the bounds of aircraft design and has reached the realm of civil engineering. The most significant criterion for laminated composite structure safety design is the failure. Failure analysis of laminated composite materials is far more complicated than failure analysis of isotropic materials. In general, the creation of laminated composite plates necessitates a thorough understanding of the damage to failure and an accurate modeling. Until now, many failure criteria have been offered in order to predict the behavior of composite structures. Tsai–Wu [1], Tsai–Hill [2], Hoffman [3],

Maximum stress [4], maximum strain [4], quadric surfaces [5] and modified quadric surfaces [6] are the most extensively utilized failure theories. They cannot forecast the failure mode of composite constructions (fiber or matrix). Failure theories such as Hashin [7], Norris [8], Hart-Smith [9], Sun [10] and Davila. [11], Puck [12] and Catalanotti [13] used these criterion to forecast fiber-dominated and matrix-dominated composite structure failures.

Tsai-Hill failure criterion directly adapts to the von-Mises criterion [14]. R. Hill introduced one of the first interactive failure criteria applicable to anisotropic materials [15, 16]. In the case of unidirectional composite materials, V.D. Azzi and S.W. Tsai [17] simplified the Hill fracture criterion in-plane stresses. In 1973, Hashin proposed two different failure criterions, the first related to fiber failure and the second to matrix failure. In order to improve the prediction capabilities of the Hachin criteria, many researchers, including Sun and Puck, have proposed some modifications [11], Sun et al. [10] proposed an amendment to the failure of matrix compression for the Hachin criteria, Puck [12, 14] proposed a three-dimensional criterion that considers the tractions interaction on the fracture plane. In the same context, Davila [11] proposed new failure criteria for polymer laminates reinforced by fiber, which are denoted LaRC03. This criterion can predict matrix and fiber failure and fracture angle (are used Mohr-Coulomb effective stresses for determining the angle of fracture plane) for matrix failure under transverse compression by maximizing the Mohr-Coulomb effective stresses. Kim et al. [18] used a finite element method with layer-wise constant shear (BLCS) under bending loads to study the progressive failure of laminated composite beams using Tsai–Wu and Maximum stress failure criteria to predict the failure at Gaussian points of each damaged beam. On the other hand, Nazargah et al. [19] developed a four-node quadrilateral partial mixed plate element with few degrees of freedom. This finite element model is based on a parametrized mixed variational concept established recently by for static and free vibration analysis of functionally graded material (FGM) plates supported by Winkler-Pasternak elastic foundations. The provided model was validated by comparing it to the results of the three-dimensional (3D) theory of elasticity as well as the results of the classical and high-order plate theories available in the literature. In addition, a high-performance finite element model for bending and vibration analysis of thick plates has been developed by Nazargah [20] based on the parametrized mixed variational principle. For the bending and vibration analysis of multi-layered composite plates, Nazargah et al. [21] presented a unique mixed-field theory with a small number of unknown variables [21]. Irhirane et al. [22] have studied bending failure for graphite-epoxy laminates. The laminate composites have been modeled using eight-node isoparametric plate bending elements using first-order shear deformation theory (FSDT). On the other hand, different failure criteria theories are used to predict damage. Moncada et al. [23] used various failure theories to study the progressive failure of laminated composites and compared the results obtained by each of them. The generalized and high-fidelity generalized of cells micromechanics method, coupled with classical laminated theory, are used. It was shown that the numerical results agree with the experimental results. In addition, Hasan et al. [24] studied the failure analysis and shape control of smart laminated composites containing different types of piezoelectric materials under coupled thermal, electrical, and mechanical stimuli. They used various failure criteria, such as Tsai-Wu, Tsai-Hill, and Maximum stress criteria, to predict the first-ply failure FPF and ultimate laminate failure. Daniel [25] proposed a new nonlinear constitutive model to describe composites' behavior and failure criteria under static and dynamic loading. M. Lezgy-Nazargah [26] investigated composite laminated beams' progressive failure analysis. The RHGB (refined high-order global-local beam) theory is used in his finite element formulation. Several failure criteria

were used to describe the failure behavior of laminated composites and predict the FPF and UFP (ultimate failure load) of composite laminates with different loads, fiber orientation, and boundary conditions.

FPF and damage location of a composite beam subjected to bending loads are investigated in this work. The FPF load is predicted using a rectangular finite element with 6 degrees of freedom at each node formulated based on the CLT. To achieve this purpose, numerous failure criteria (Maximum Stress, Tsai-Hill, Tsai-Wu, and Hashin's criterion) are used to predict failure mechanisms.

FINITE ELEMENT FORMULATION

Based on Kirchhoff assumptions, the displacement field [27, 28] according to the CLT is given by the following equations:

$$\begin{aligned} u(x,y,z) &= u_0(x,y) - z\frac{\partial w}{\partial x} \\ v(x,y,z) &= v_0(x,y) - z\frac{\partial w}{\partial y} \\ w(x,y,z) &= w_0(x,y) \end{aligned} \tag{1}$$

where u_0, v_0 and w_0 are the mid-plane displacement components of the plate element. The strain-displacement relations can be expressed as

$$\begin{aligned} \varepsilon_x &= \frac{\partial u}{\partial x} = -z\frac{\partial^2 w}{\partial^2 x} = zk_x \\ \varepsilon_y &= \frac{\partial v}{\partial y} = -z\frac{\partial^2 w}{\partial^2 y} = zk_y \\ 2\varepsilon_{xy} &= \frac{\partial u}{\partial y} + \frac{\partial v}{\partial x} = -2z\frac{\partial^2 w}{\partial x \partial y} = zk_{xy} \end{aligned} \tag{2}$$

By adopting the classical laminate assumptions, the resultant forces *N* and moments *M* are related to the mid-surface strains ε^0 and to the curvatures *k* by:

$$\begin{Bmatrix} N \\ M \end{Bmatrix} = \begin{bmatrix} A & B \\ B & D \end{bmatrix} \begin{Bmatrix} \varepsilon^0 \\ k \end{Bmatrix} \tag{3}$$

Where the matrices [*A*], [*B*], and [*D*] are known as extensional, coupling, and bending rigidity matrices, respectively. These rigidities can be defined by:

$$\{A, B, D\}^T = \int_{-h/2}^{+h/2} \left[\bar{Q}_{ij}\right](1, z, z^2)dz \tag{4}$$

With $\bar{Q}_{ij}$ denoting the coefficients of elasticity of a layer in the global coordinate system (*x*, *y*, *z*) of the laminate forming an angle θ with the local coordinate system. The finite element used in this investigation is a rectangular element of 24 degrees of freedom per element. Figure 1 shows the geometry of the present element.

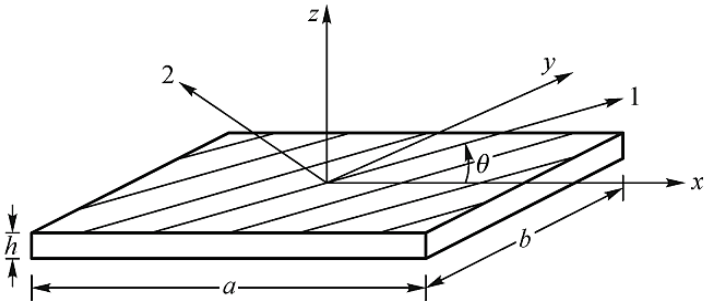


Fig. 1. Geometry and coordinate systems of the rectangular laminated plate

The current element has four (4) nodes, each with six degrees of freedom. The nodal degrees of freedom of the present element are

$$\{q\} = \left\{ u_i, v_i, w_i, \frac{\partial w_i}{\partial x}, \frac{\partial w_i}{\partial y}, \frac{\partial^2 w_i}{\partial x \partial y} \right\}_{i=1,4}$$

The presented element is a combination of a membrane element and a rectangular plate element with a high degree of accuracy. The membrane displacement of the developed element, through the element, can be expressed in terms of the interpolation functions as

$$\begin{Bmatrix} u(x,y) \\ v(x,y) \end{Bmatrix} = \begin{bmatrix} -\frac{x}{a} - \frac{y}{b} + \frac{xy}{ab} + 1 & 0 & \frac{x}{a} - \frac{xy}{ab} & 0 & \frac{xy}{ab} & 0 & \frac{y}{b} - \frac{xy}{ab} & 0 \\ 0 & -\frac{x}{a} - \frac{y}{b} + \frac{xy}{ab} + 1 & 0 & \frac{x}{a} - \frac{xy}{ab} & 0 & \frac{xy}{ab} & 0 & \frac{y}{b} - \frac{xy}{ab} \end{bmatrix} \left\{ \delta_m^e \right\} \tag{5}$$

Where $\left\{\delta_m^e\right\}$ is the membrane displacement vector of the element. The Eq. 5 can be written as

$$\begin{Bmatrix} u(x,y) \\ v(x,y) \end{Bmatrix} = \begin{bmatrix} N_1^m & 0 & N_2^m & 0 & N_3^m & 0 & N_4^m & 0 \\ 0 & N_1^m & 0 & N_2^m & 0 & N_3^m & 0 & N_4^m \end{bmatrix} \left\{ \delta_m^e \right\} \tag{6}$$

The interpolation functions can be used to express the membrane strain-displacement relation as

$$\{\varepsilon(x,y)\} = [B_m]\{\delta_m^e\} \tag{7}$$

$$[B_m] = \begin{bmatrix} \frac{\partial N_1^m}{\partial x} & 0 & \frac{\partial N_2^m}{\partial x} & 0 & \frac{\partial N_3^m}{\partial x} & 0 & \frac{\partial N_4^m}{\partial x} & 0 \\ 0 & \frac{\partial N_1^m}{\partial y} & 0 & \frac{\partial N_2^m}{\partial y} & 0 & \frac{\partial N_3^m}{\partial y} & 0 & \frac{\partial N_4^m}{\partial y} \\ \frac{\partial N_1^m}{\partial y} & \frac{\partial N_1^m}{\partial x} & \frac{\partial N_2^m}{\partial y} & \frac{\partial N_2^m}{\partial x} & \frac{\partial N_3^m}{\partial y} & \frac{\partial N_3^m}{\partial x} & \frac{\partial N_4^m}{\partial y} & \frac{\partial N_4^m}{\partial x} \end{bmatrix} \tag{8}$$

The transverse displacement *w* of the element is expressed as

$$w(x,y) = \begin{bmatrix} \alpha_1 + \alpha_2 x + \alpha_3 y + \alpha_4 x^2 + \alpha_5 xy + \alpha_6 y^2 + \alpha_7 x^3 + \alpha_8 x^2 y + \alpha_9 xy^2 + \alpha_{10} y^3 + \alpha_{11} x^3 y + \\ \alpha_{12} x^2 y^2 + \alpha_{13} xy^3 + \alpha_{14} x^3 y^2 + \alpha_{15} x^2 y^3 + \alpha_{16} x^3 y^3 \end{bmatrix} \tag{9}$$

The displacement function of the plate element, given by Eq. (9), can be written in a vector form as

$$w(x,y) = \{P(x,y)\}\{\alpha\}^T \tag{10}$$

With $w(x,y)$ is the displacement function of the plate element and $\{\alpha\}^T$ is the constant parameters vector. As the plate element requires four degrees of freedom per node,

$$\delta_f^e = \left\{ w_i, \theta_{xi} = \frac{\partial w_i}{\partial x}, \theta_{yi} = \frac{\partial w_i}{\partial y}, \theta_{xyi} = \frac{\partial^2 w_i}{\partial x \partial y} \right\}_{i=1,4}$$

The plate displacements through the element can be expressed in terms of the nodal displacements as

$$w(x,y) = \{P(x,y)\}_{1\times 16} [X]^{-1}_{16\times 16} \{\delta_f^e\}_{16\times 1} \tag{11}$$

So

$$w(x,y) = \begin{bmatrix} N_1^f & N_2^f & N_3^f & N_4^f & . & . & . & . & . & . & . & . & N_{13}^f & N_{14}^f & N_{15}^f & N_{16}^f \end{bmatrix} \{\delta_f^e\} \tag{12}$$

Where the interpolation functions of the plate element are written as

$$w^*_1(x,y) = (1-3\frac{x^2}{a^2}+2\frac{x^3}{a^3})(1-3\frac{y^2}{b^2}+2\frac{y^3}{b^3})w_1 + (-x(\frac{x}{a}-1)^2)(1-3\frac{y^2}{b^2}+2\frac{y^3}{b^3})\theta_{x1} + (1-3\frac{x^2}{a^2}+2\frac{x^3}{a^3})y(\frac{y}{b}-1)^2\theta_{y1} +$$
$$(-x(\frac{x}{a}-1)^2)y(\frac{y}{b}-1)^2\theta_{xy1}$$

$$w^*_2(x,y) = (3\frac{x^2}{a^2}-2\frac{x^3}{a^3})(1-3\frac{y^2}{b^2}+2\frac{y^3}{b^3})w_2 + (-x(\frac{x^2}{a^2}-\frac{x}{a}))(1-3\frac{y^2}{b^2}+2\frac{y^3}{b^3})\theta_{x2} + (3\frac{x^2}{a^2}-2\frac{x^3}{a^3})y(\frac{y}{b}-1)^2\theta_{y2} +$$
$$(-x(\frac{x^2}{a^2}-\frac{x}{a}))y(\frac{y}{b}-1)^2\theta_{xy2}$$

$$w^*_3(x,y) = (3\frac{x^2}{a^2}-2\frac{x^3}{a^3})(3\frac{y^2}{b^2}-2\frac{y^3}{b^3})w_3 + (-x(\frac{x^2}{a^2}-\frac{x}{a}))(3\frac{y^2}{b^2}-2\frac{y^3}{b^3})\theta_{x3} + (3\frac{x^2}{a^2}-2\frac{x^3}{a^3})y(\frac{y^2}{b^2}-\frac{y}{b})\theta_{y3} +$$
$$(-x(\frac{x^2}{a^2}-\frac{x}{a}))y(\frac{y^2}{b^2}-\frac{y}{b})\theta_{xy3}$$

$$w^*_4(x,y) = (1-3\frac{x^2}{a^2}+2\frac{x^3}{a^3})(3\frac{y^2}{b^2}-2\frac{y^3}{b^3})w_4 + (-x(\frac{x}{a}-1)^2)(3\frac{y^2}{b^2}-2\frac{y^3}{b^3})\theta_{x4} + (1-3\frac{x^2}{a^2}+2\frac{x^3}{a^3})y(\frac{y^2}{b^2}-\frac{y}{b})\theta_{y4} +$$
$$(-x(\frac{x}{a}-1)^2)y(\frac{y^2}{b^2}-\frac{y}{b})\theta_{xy4} \tag{13}$$

Kinematics relation

The present element is based on the CLT, so the in-plane and out-of-plane displacements are given using eq. (1). On the other hand, based on the strain-displacement relation, the curvatures *k* can be given as

$$\{k(x,y)\} = -\begin{Bmatrix} \frac{\partial^2 w}{\partial x^2} \\ \frac{\partial^2 w}{\partial y^2} \\ 2\frac{\partial^2 w}{\partial x \partial y} \end{Bmatrix} = -\begin{bmatrix} \frac{\partial^2}{\partial x^2} \\ \frac{\partial^2}{\partial y^2} \\ 2\frac{\partial^2}{\partial x \partial y} \end{bmatrix} \{P(x,y)\}[X]^{-1}\{\delta_f^e\} = -\begin{bmatrix} \frac{\partial^2 \{P(x,y)\}}{\partial x^2} \\ \frac{\partial^2 \{P(x,y)\}}{\partial y^2} \\ 2\frac{\partial^2 \{P(x,y)\}}{\partial x \partial y} \end{bmatrix} [X]^{-1}\{\delta_f^e\}$$

$$\{k(x,y)\} = [Q]_{3\times 16}[X]^{-1}_{16\times 16}\{\delta_f^e\}_{16\times 1} = [B_f]_{3\times 16}\{\delta_f^e\} \tag{14}$$

The total potential energy of deformation of a plate subjected to a distributed transverse loading is given by:

$$\Pi = U + V' \tag{15}$$

The equilibrium configuration is defined by the minimization of the total potential energy which means the cancellation of its first variation.

$$\delta\Pi = \delta U + \delta V = 0 \tag{16}$$

The element stiffness matrix $\left[K^e\right]$ can be obtained as

$$\left[K^e\right] = \iint \left\{ [B_m]^T [A][B_m] + [B_m]^T [B][B_f] + [B_f]^T [B][B_m] + [B_f]^T [D][B_f] \right\} ds \tag{17}$$

Strain and stresses in a laminated beam

A computer program is prepared for calculating local strains and stress distributions in a laminated beam, subjected to the applied forces and moments, using the steps listed below:

1- Calculate the values of the reduced stiffness matrix [*Q*] for each ply using its four elastic moduli, E_1, E_2, ν_{12} and G_{12}.

2- Use the [*Q*] matrix produced in step 1 and the ply angle to determine the value of the transformed global reduced stiffness matrix $\left[\bar{Q}_{ij}\right]$ for each ply.

3- Knowing the thickness t_k, of each layer, find the coordinates of the top and bottom of each layer h_i, $i = 1\ldots, n$, and the total thickness h of the laminate using the following equations

$$h = \sum_{k=1}^{n} t_k \tag{18}$$

4- The location of the mid-plane is *h*/2 from the top or the bottom surface of the laminate. The *z*-coordinate of each ply *k* surface (top and bottom) is given by

- Ply 1:

$$h_0 = -h/2 \text{ (top surface)}$$
$$h_1 = -h/2 + t_1 \text{ (bottom surface).}$$

- Ply *k*: (*k*= 2, 3,.., *n*-2, *n*-1)

$$h_{k-1} = -h/2 + \sum_{=1}^{k-1} t \text{ (top surface).}$$
$$h_k = -h/2 + \sum_{=1}^{k} t \text{ (bottom surface).}$$

- Ply *n*:

$$h_{n-1} = h/2 - t_n \text{ (top surface).}$$
$$h_n = h/2 \text{ (bottom surface).}$$

5- Using the matrix from step 2 and the position of each layer from step 3, to calculate the three stiffness matrices [*A*], [*B*], and [*D*] using Eq. 4.

6- Substitute the stiffness matrix values found in step 4 and the applied forces and moments in Eq. 3.

7- Solve the six simultaneous equations, Eq. 3, to find the mid-plane strains and curvatures.

8- Now that the position of each layer is known, find the global strain in each layer using the following expression

$$\begin{Bmatrix} \varepsilon_x \\ \varepsilon_y \\ \gamma_{xy} \end{Bmatrix} = \begin{Bmatrix} \varepsilon_x^0 \\ \varepsilon_y^0 \\ \gamma_{xy}^0 \end{Bmatrix} + z \begin{Bmatrix} k_x \\ k_y \\ k_{xy} \end{Bmatrix} \tag{19}$$

9- To find the global stresses in each lamina, use the following stress-strain expression:

$$\begin{Bmatrix} \sigma_x \\ \sigma_y \\ \tau_{xy} \end{Bmatrix} = \left[\overline{Q_{ij}}\right] \begin{Bmatrix} \varepsilon_x \\ \varepsilon_y \\ \gamma_{xy} \end{Bmatrix} \tag{20}$$

10- To find the local strains, use the following transformation equation:

$$\begin{Bmatrix} \varepsilon_1 \\ \varepsilon_2 \\ \gamma_{12}/2 \end{Bmatrix} = [T]^{-1} \begin{Bmatrix} \varepsilon_x \\ \varepsilon_y \\ \gamma_{xy}/2 \end{Bmatrix} \tag{21}$$

11- For finding the local stresses, use following the transformation equation

$$\begin{Bmatrix} \sigma_1 \\ \sigma_2 \\ \tau_{12} \end{Bmatrix} = [T]^{-1} \begin{Bmatrix} \sigma_x \\ \sigma_y \\ \tau_{xy} \end{Bmatrix} \tag{22}$$

FAILURE CRITERION

As mentioned previously, the main objective of this study is to determine the failure load of laminated beams subjected to various bending conditions. Three different families of failure criteria are adopted in this investigation. The first is the maximum stress criterion (there is no interaction between the lamina stresses). The second criteria are Tsai-Hill and Tsai-Wu (there is an interaction between the lamina stresses). The last one is the Hashin criterion.

Maximum stress failure criterion

The maximum stress failure criterion has the advantage of being simple in form and easy to apply, but this criterion ignores the interactions between different stress components (one can assume that there is no interaction between stresses or strain components). If one of the following conditions is verified, failure initiation begins.

$$\frac{\sigma_1}{X_t}=1 \text{ for } \sigma_1>0 \text{ and } \frac{\sigma_1}{X_c}=1 \text{ for } \sigma_1<0;$$
$$\frac{\sigma_2}{Y_t}=1 \text{ for } \sigma_2>0 \text{ and } \frac{\sigma_2}{Y_c}=1 \text{ for } \sigma_2<0;$$
$$\frac{|\tau_{12}|}{S}=1 \tag{23}$$

where σ_1, σ_2 and τ_{12} are the ply normal and shear stress components, X_t and X_c are the longitudinal strengths in tension and compression, respectively. Y_t and Y_c are the transverse strengths in tension and compression, respectively. *S* is the in-plane shear strength.

Tsai-Hill quadratic failure criterion

Tsai-Hill failure criterion directly adapts to the classic Von-Mises criterion [14]. Then, Tsai and Hill made some modifications to apply this criterion to anisotropic materials. Contrary to the maximum stress criterion, this failure criterion considers the interaction between the stress components.

$$\left(\frac{\sigma_1}{X}\right)^2+\left(\frac{\sigma_2}{Y}\right)^2-\frac{\sigma_1\sigma_2}{X^2}+\left(\frac{\tau_{12}}{S}\right)^2=1 \tag{24}$$

Tsai–Wu failure criterion

The Tsai-Wu failure criterion is widely used in anisotropic materials and is based on the total strain energy failure theory [28]. This criterion takes account of the interaction between stresses. When a laminate's failure index approaches 1, the Tsai-Wu criterion predicts failure.

$$F_i\sigma_i+F_{ij}\sigma_i\sigma_j\geq 1, \quad i,j=1,2,...,6 \tag{25}$$

Based on this criterion, the failure load can be calculated using the following expression:

$$\sigma f_1\left(\frac{\sigma_1}{\sigma}\right)+\sigma f_2\left(\frac{\sigma_2}{\sigma}\right)+\sigma^2 f_{11}\left(\frac{\sigma_1}{\sigma}\right)^2+\sigma^2 f_{22}\left(\frac{\sigma_2}{\sigma}\right)^2+\sigma^2 f_{66}\left(\frac{\sigma_{12}}{\sigma}\right)^2+2\sigma^2 f_{12}\left(\frac{\sigma_1\sigma_2}{\sigma^2}\right)=1 \tag{26}$$

By designating the value of σ that causes failure as σ_f, Eq. 26 can be rewritten as:

$$A\sigma_f^2+B\sigma_f-1=0 \tag{27}$$

Where

$$A=f_{11}\left(\frac{\sigma_1}{\sigma}\right)^2+f_{22}\left(\frac{\sigma_2}{\sigma}\right)^2+f_{66}\left(\frac{\sigma_{12}}{\sigma}\right)^2+2f_{12}\left(\frac{\sigma_1\sigma_2}{\sigma^2}\right)$$
$$B=f_1\left(\frac{\sigma_1}{\sigma}\right)+f_2\left(\frac{\sigma_2}{\sigma}\right)$$
$$f_{11}=\frac{1}{X_tX_c}, \quad f_{22}=\frac{1}{Y_tY_c}, \quad f_{66}=\frac{1}{S^2},$$
$$f_1=\frac{1}{X_t}-\frac{1}{X_c}, \quad f_2=\frac{1}{Y_t}-\frac{1}{Y_c}, \; f_{12}\cong -0.5(f_{11}f_{22})^{1/2} \tag{28}$$

Hashin failure criterion

The Hashin criterion is a failure criterion that is physically based. This criterion can predict the failure modes and mechanisms of unidirectional composites. It is based on four main modes of material failure, as presented in Table 1.

Table 1. *Failure modes based on Hashin criterion*

Failure modes	Mathematical expression
Fiber failure in tension $\sigma_{11} > 0$	$\left(\frac{\sigma_{11}}{X_t}\right)^2 + \left(\frac{\tau_{12}}{S}\right)^2 \geq 1$
Fiber failure in compression $\sigma_{11} < 0$	$\left(\frac{\sigma_{11}}{X_c}\right)^2 \geq 1$
Matrix failure in tension $\sigma_{22} > 0$	$\left(\frac{\sigma_{22}}{Y_t}\right)^2 + \left(\frac{\tau_{12}}{S}\right)^2 \geq 1$
Matrix failure in compression $\sigma_{22} < 0$	$\left(\frac{\sigma_{22}}{Y_c}\right)^2 + \left(\frac{\tau_{12}}{S}\right)^2 \geq 1$

RESULTS AND DISCUSSION

In order to assess the performance of the present element to convergence, various examples are studied considering symmetric laminated beams with different stacking sequences, different loadings, geometry, and boundary conditions. The numerical results obtained are compared with analytical solutions and other numerical results found in literature based on high-order finite element models. Before beginning this examination, a convergence study of the current element should be performed to ensure that the present finite element performs. The obtained results are extracted from FORTRAN and MATLAB codes written by the authors based on the proposed formulations mentioned in the preceding sections.

Example 1*: Simply supported cross-ply laminated beam* $[90_2/0]_s$ *under a concentrated load*

In the first example, a simply supported (*SS*) six-layer laminated beam subjected to a concentrated load P=100 kN is considered (see Figure 2). The concentrated load is applied at the mid-span of the beam (three-point bending test). The thickness of each layer is 2 mm.

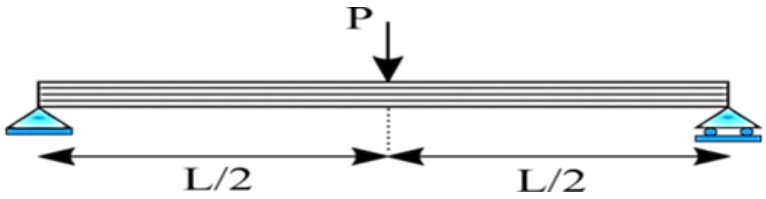


Fig. 2. Simply supported laminated beam $[90_2/0]_s$ under a concentrated load

The geometric and the mechanical characteristics of the laminated beam are presented in Table 2.

Table 2. *Geometrical parameters and mechanical proprieties*

E_1 (MPa)	E_2 (MPa)	G_{12} (MPa)	ν_{12}	P (kN)	*Length L* (mm)	*Width b* (mm)	*Thickness h* (mm)
$123x10^7$	8.5×10^7	4.1×10^7	0.25	100	1000	200	12

The numerical results obtained by the present element are compared with the analytical solution. The maximum value of the analytical displacement is calculated using the following relation

$$w = \frac{PL^3}{48E_{eq}I} \tag{29}$$

with

$$E_{eq} = 12 \diagup D_{11}h^3$$

The convergence of the transverse displacement, using different mesh sizes, is shown in Table 3.

Table 3. *Displacement convergence of a simply supported beam subjected to a concentrated load*

Mesh size	4×2	8×4	10×4	12×6	20×8	40×8	Analytical displacement
Displacement	0.56671	0.56676	0.56677	0.56678	0. 5668	0.56681	0.567
Error (%)	$5.114E^{-2}$	$4.232E^{-2}$	$4.056E^{-2}$	$3.880E^{-2}$	$3.52E^{-2}$	$3.35E^{-2}$	-

As can be observed, the current finite element has a high convergence rate. By using only 10×4 elements, it is almost adequate to determine the maximum deflection of the laminated beam with enough engineering accuracy. In addition, for mesh size (40×8) elements, the error percentage of the transverse displacement predicted by employed element is around 3.35E-2% compared to the analytical solution. Based on prior convergence studies, it is clear that (40 × 8) elements are most sufficient to get more precise results. Therefore, all the subsequent results are obtained using (40×8) elements.

***Example 2**: FPF analysis of a simply supported cross-ply $[90_8/0_8]_s$ beams*

The second example is considered in order to verify the present element's ability and validity in predicting the FPF strength of beams with various geometrical parameters. In this example, the FPF load and its corresponding displacement of cross-ply laminated beams $[90_8/0_8]_s$ are predicted using the present element. The analyzed beams are *SS*, and a concentrated load is applied at the mid-span of the beams. The laminated beams are made of graphite/epoxy and the material characteristics, geometrical, and strength parameters are listed in Table 4.

***Table 4.** Geometric and material properties of AS4/3502 graphite/epoxy*

E_1 (MPa)	E_2 (MPa)	G_{12} (MPa)	ν_{12}	X_t (MPa)	X_c (MPa)	Y_t (MPa)	Y_c (MPa)	S (MPa)
141200	11500	6000	0.3	2343	1723	51	223	86
Laminate	*Length L* (mm)	*Width b* (mm)	*Thickness h* (mm)	Lay-up				
A1	139.7	24.84	4.648	$[90_8/0_8]_s$				
A2	152.4	25.65	4.547	$[90_8/0_8]_s$				

The FPF analysis of the considered beams has also been examined by M. L. Nazargah [26] using a high-order global-local (HO-GL) finite element model, Kim et al. [18] using a beam finite element with LW constant shear, and the analytical results obtained by the CLT. One can see in Tables 5 and 6 that, by using different failure criteria, the predicted FPF loads and their corresponding deflections produced by the current element are in good agreement with the numerical and analytical results. Therefore, the performance of the developed element is confirmed both in terms of good accuracy and a quick rate of convergence.

***Table 5.** FPF load (N) of the laminated graphite/epoxy beams*

Failure criteria	Analytical results based on CLT	Numerical results based on HO-GL model [26]	Numerical results based on LW theory [18].	Numerical results based on Present element
A1				
Hashin	325	303	-	356
Maximum Stress	325	304	307	356
Tsai-Hill	325	304	-	356
Tsai-Wu	327	304	307	361
A2				
Hashin	295	274	-	325
Maximum Stress	295	275	307	325
Tsai-Hill	295	275	-	325
Tsai-Wu	297	275	307	329

Table 6. *Displacement (mm) using FPF load of the laminated graphite/epoxy beams*

Failure criteria	Analytical results based on CLT	Numerical results based on Present element
A1		
Hashin	3.210	3.513
Maximum Stress	3.210	3.513
Tsai-Hill	3.210	3.513
Tsai-Wu	3.229	3.562
A2		
Hashin	3.900	4.293
Maximum Stress	3.900	4.293
Tsai-Hill	3.900	4.293
Tsai-Wu	3.927	4.346

Parametric study

After establishing the accuracy of the present element, a comprehensive analysis of bending, and damage of multilayered beams is carried out. The effects of loading, boundary conditions, number of layers, and stacking sequences are investigated and discussed in detail. The following analysis is focused on glass/epoxy beams using the present element, and the results are compared to the analytical solution based on the CLT.

Effect of loading and boundary conditions on the FPF strength

After validating the performance of the presented elements for the analysis of cross-laminated beams, this section considers a number of numerical tests to study the transverse deformation and FPF strength. Table 7 presents both loading and boundary conditions, for which the numerical results are obtained, where CC, SS, and CF respectively indicate: fully clamped, fully simply supported, and clamped from one side and free from the other, respectively.

The laminated beams are made of glass/epoxy, and their corresponding geometrical and material characteristics are given in Table 8.

Table 7. *Boundary conditions used in the numerical tests*

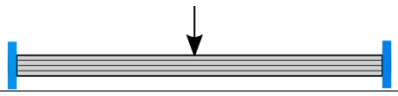
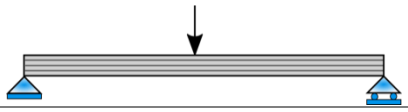
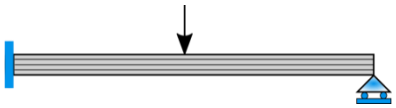
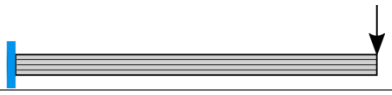
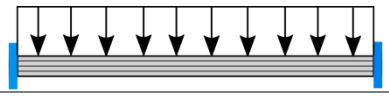
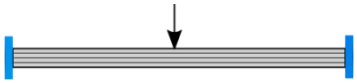
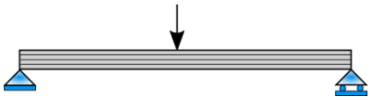
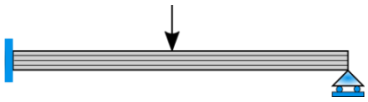
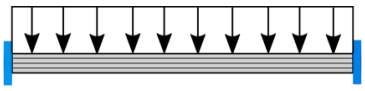
Abbreviations	Restrained edges	
CC	$u=0, v=0, w=0, \frac{\partial w}{\partial x}=0, \frac{\partial w}{\partial y}=0, \frac{\partial^2 w}{\partial x \partial y}=0$	
SS	$u\neq 0, v\neq 0, w=0, \frac{\partial w}{\partial x}\neq 0, \frac{\partial w}{\partial y}=0, \frac{\partial^2 w}{\partial x \partial y}\neq 0$	
CS	$u=0, v=0, w=0, \frac{\partial w}{\partial x}=0, \frac{\partial w}{\partial y}=0, \frac{\partial^2 w}{\partial x \partial y}=0$ $u\neq 0, v\neq 0, w=0, \frac{\partial w}{\partial x}\neq 0, \frac{\partial w}{\partial y}=0, \frac{\partial^2 w}{\partial x \partial y}\neq 0$	
CF	$u=0, v=0, w=0, \frac{\partial w}{\partial x}=0, \frac{\partial w}{\partial y}=0, \frac{\partial^2 w}{\partial x \partial y}=0$	
CC with two concentrated loads	$u=0, v=0, w=0, \frac{\partial w}{\partial x}=0, \frac{\partial w}{\partial y}=0, \frac{\partial^2 w}{\partial x \partial y}=0$	
CC with a distributed load	$u=0, v=0, w=0, \frac{\partial w}{\partial x}=0, \frac{\partial w}{\partial y}=0, \frac{\partial^2 w}{\partial x \partial y}=0$	

Table 8. *Geometric and material properties of glass/epoxy beams*

E_1 (MPa)	E_2 (MPa)	G_{12} (MPa)	ν_{12}	X_t (MPa)	X_c (MPa)	Y_t (MPa)	Y_c (MPa)	S (MPa)
141000	9340	4500	0.35	1500	1000	180	240	150
Laminate	*Length L* (mm)	*Width b* (mm)	*Thickness h* (mm)	Lay-up				
A3	1000	100	2	$[0/90]_s$				

Table 9 presents the comparisons of maximum transverse displacement and FPF loads of glass/epoxy laminated beams using various failure criteria.

Table 9. *Displacement (mm) and FPF load (N) of glass/epoxy laminated beams*

Boundary condition	Failure theory	Displacement		FPF load	
		Analytical results based on CLT	Numerical results based on present element	Analytical results based on CLT	Numerical results based on present element
	Tsai-Wu	305.44	300.92	490.00	482.00
	Hashin	284.87	287.22	457.00	489.00
	Max Stress	284.87	242.89	457.00	389.00
	Tsai-Hill	286.74	242.89	460.00	389.00
	Tsai-Wu	649.40	611.52	260.00	245.00
	Hashin	606.94	534.15	243.00	214.00
	Max Stress	606.94	534.15	243.00	214.00
	Tsai-Hill	609.44	536.65	244.00	215.00
	Tsai-Wu	2515.52	2436.60	63.00	61.00
	Hashin	2315.88	2276.90	58.00	57.00
	Max Stress	2315.88	2316.80	58.00	58.00
	Tsai-Hill	2355.81	2316.80	59.00	58.00
	Tsai-Wu	365.06	360.38	327.00	330.00
	Hashin	340.50	334.19	305.00	306.00
	Max Stress	340.50	352.76	305.00	323.00
	Tsai-Hill	342.73	336.38	307.00	308.00
	Tsai-Wu	235.54	238.71	291.00	295.00
	Hashin	219.35	212.25	271.00	278.00
	Max Stress	219.35	239.74	271.00	314.00
	Tsai-Hill	220.97	213.01	273.00	279.00
	Tsai-Wu	237.48	234.55	0.0076	0.007
	Hashin	221.86	217.80	0.0071	0.0065
	Max Stress	221.86	237.90	0.0071	0.0071
	Tsai-Hill	221.86	217.80	0.0071	0.0065

On the other hand, the transverse deflection distributions of glass-epoxy laminated beams using various boundary conditions are presented in Figure 3.

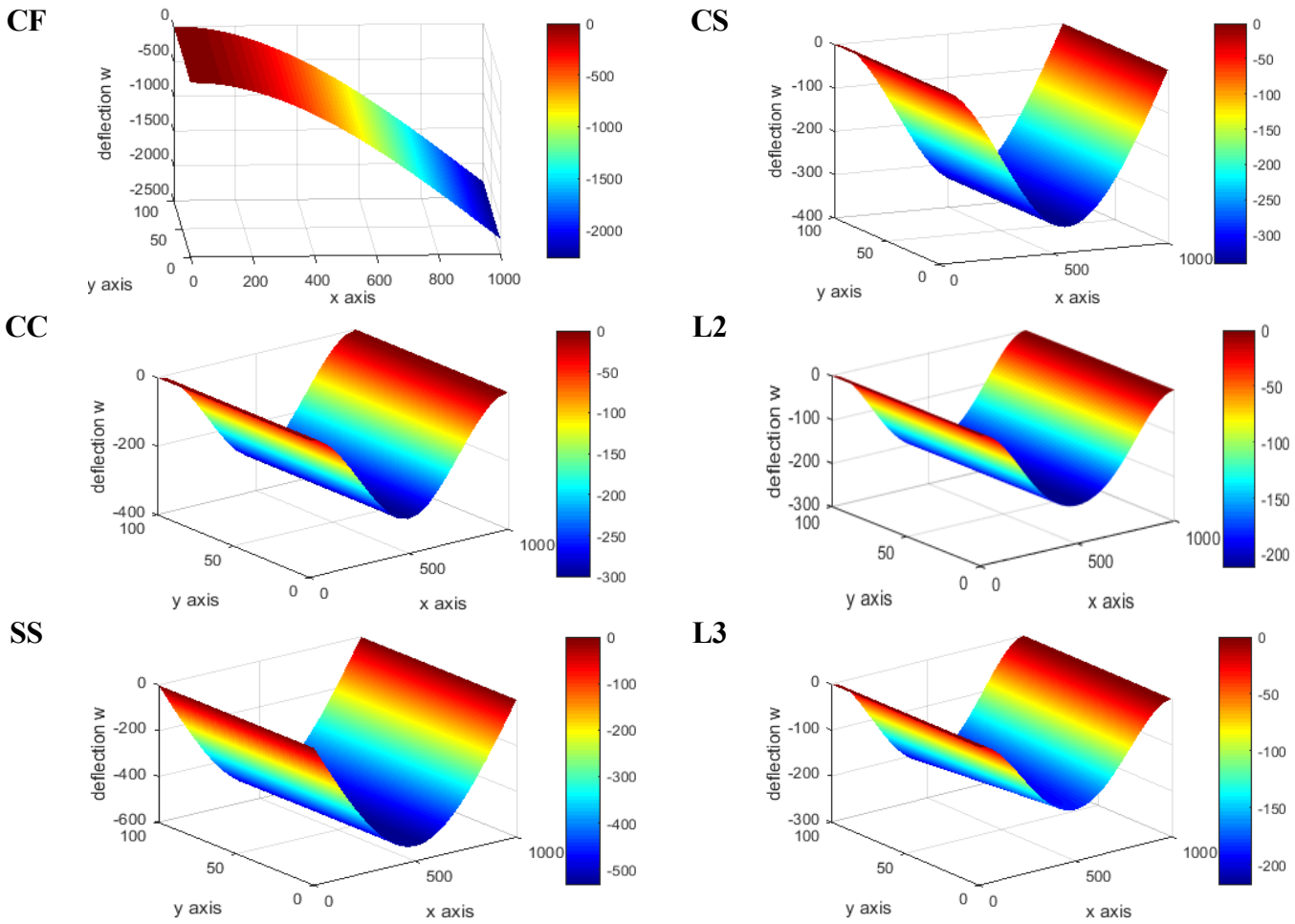


Fig. 3. The transverse displacement distribution of FPF for different boundary conditions in glass-epoxy laminated beams (L2: CC with tow concentrated loads and L3: CC with distributed load)

The numerical results are obtained for various schemes of loading and different boundary conditions. These results are compared to those obtained by the analytical solution based on the CLT.

As can be seen in Table 9, for both displacement and FPF load results, there are no significant differences between the present results and the analytical solutions. For example, by using the Tsai-Wu failure theory, the maximum displacements obtained by the present element and CLT are almost the same, and they equal 300.92 mm and 305.44 mm, respectively. On the other hand, by considering the same example, the predicted FPF loads obtained using the Hashin criterions are 460.00 N and 457.00 N, respectively. Moreover, it can be observed that the BC and loading have a remarkable impact on the FPF loads.

Effect of stacking sequences on the FPF strength and deflection of FPF

In the present section, clamped and simply supported glass/epoxy multilayered beams are studied. The computational results are obtained for various symmetric stacking sequences. Two different configurations of stacking sequences, $[0°/\theta°]_s$ and $[90°/\theta°]_s$, are considered to see the direct effect of fiber orientation on FPF load and deflection of FPF. Furthermore, by using

Hashin criterion, the damage mechanism and location can easily be detected. Tsai-Wu criterion is also adopted for comparison purpose. In these examples, we kept the same geometrical and mechanical properties of the previous beams and changing only fiber orientation and the support conditions.

The FPF results of glass/epoxy beams subjected to a concentrated load at the mid-span of the beams are highlighted in Tables 10, 11 and Figures 4 and 5. Tables 12, 13 and Figures 6 and 7 show the transverse deformation caused by the FPF load of glass/epoxy beams.

Table 10. *FPF loads (N) of clamped and simply supported [0°/θ°]s glass/epoxy beams*

BC	Lay-up	Tsai-Wu criteria		Hashin criteria		
		Analytical results based on CLT	Numerical results based on the present element	Analytical results based on CLT	Numerical results based on the present element	
					Load	Dominant Failure Mode Type
CC	$[0°/0°]_s$	547.0	542.0	510.0	407.0	Fiber compression
	$[0°/15°]_s$	506.0	503.0	471.0	401.0	Interface
	$[0°/30°]_s$	477.0	475.0	444.0	393.0	interface
	$[0°/45°]_s$	478.0	475.0	446.0	389.0	interface
	$[0°/60°]_s$	484.0	480.0	451.0	388.0	interface
	$[0°/75°]_s$	488.0	482.0	455.0	389.0	interface
	$[0°/90°]_s$	490.0	482.0	457.0	389.0	Fiber compression
SS	$[0°/0°]_s$	284.0	269.0	270.0	231.0	Fiber compression
	$[0°/15°]_s$	271.0	258.0	265.0	228.0	Fiber compression
	$[0°/30°]_s$	252.0	243.0	254.0	221.0	Fiber compression
	$[0°/45°]_s$	246.0	237.0	246.0	215.0	Fiber compression
	$[0°/60°]_s$	251.0	239.0	243.0	213.0	Fiber compression
	$[0°/75°]_s$	257.0	243.0	243.0	213.0	Fiber compression
	$[0°/90°]_s$	260.0	245.0	243.0	214.0	Fiber compression

Table 11. *FPF loads (N) of clamped and simply supported [90°/θ°]s glass/epoxy beams*

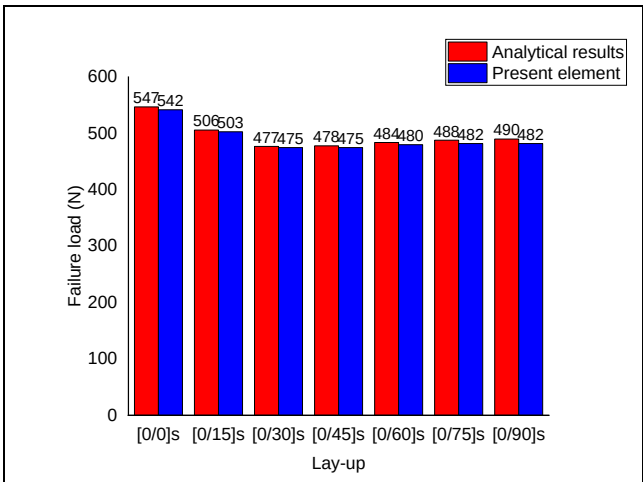
BC	Lay-up	Tsai-Wu criteria		Hashin criteria		
		Analytical results based on CLT	Numerical results based on the present element	Analytical results based on CLT	Numerical results based on the present element	
					Load	Dominant Failure Mode Type
CC	$[90°/0°]_s$	207.0	206.0	193.0	186.0	Fiber compression
	$[90°/15°]_s$	148.0	142.0	137.0	131.0	Fiber compression
	$[90°/30°]_s$	130.0	121.0	121.0	111.0	Fiber compression
	$[90°/45°]_s$	107.0	98.0	100	94.0	Matrix tensile
	$[90°/60°]_s$	97.0	95.0	92.0	90.0	Matrix tensile
	$[90°/75°]_s$	98.0	98.0	94.0	92.0	Matrix tensile
	$[90°/90°]_s$	99.0	97.0	95.0	93.0	Matrix tensile
SS	$[90°/0°]_s$	109.0	104.0	102.0	95.0	Fiber compression
	$[90°/15°]_s$	111.0	106.0	103.0	96.0	Interface
	$[90°/30°]_s$	87.0	82.0	88.0	83.0	Matrix tensile
	$[90°/45°]_s$	65.0	62.0	66.0	63.0	Matrix tensile
	$[90°/60°]_s$	53.0	51.0	54.0	52.0	Matrix tensile
	$[90°/75°]_s$	50.0	49.0	50.0	48.0	Matrix tensile
	$[90°/90°]_s$	51.0	49.0	50.0	48.0	Matrix tensile

Table 12. *Deflection of clamped and simply supported [0°/θ°]s glass/epoxy beams*

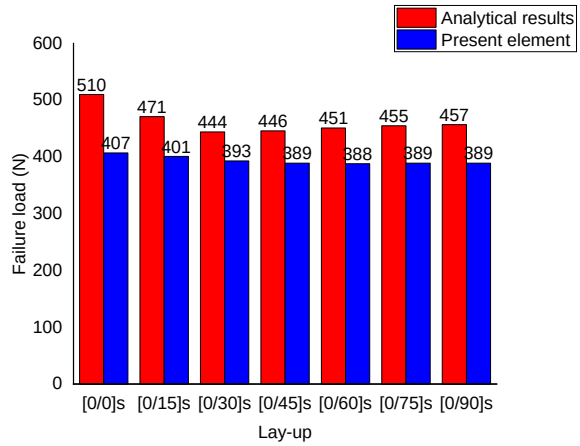
BC	Lay-up	Tsai-Wu criteria		Hashin criteria	
		Analytical results based on CLT	Numerical results based on the present element	Analytical results based on CLT	Numerical results based on the present element
CC	$[0°/0°]_s$	301.983	299.92	281.557	225.25
	$[0°/15°]_s$	286.829	285.94	266.989	227.99
	$[0°/30°]_s$	283.879	282.89	264.240	234.11
	$[0°/45°]_s$	293.687	292.02	274.026	239.22
	$[0°/60°]_s$	301.156	299.110	280.622	241.82
	$[0°/75°]_s$	304.230	301.00	283.675	243.00
	$[0°/90°]_s$	305.437	300.92	284.866	242.89
SS	$[0°/0°]_s$	629.087	595.23	598.076	511.16
	$[0°/15°]_s$	614.999	584.27	601.383	516.34
	$[0°/30°]_s$	601.368	578.19	606.141	525.86
	$[0°/45°]_s$	609.634	585.81	609.634	531.45
	$[0°/60°]_s$	629.137	597.82	609.085	532.79
	$[0°/75°]_s$	643.149	607.38	608.114	532.40
	$[0°/90°]_s$	649.400	611.52	606.940	534.15

Table 13. *Deflection of clamped and simply supported [90°/θ°]s glass/epoxy beams*

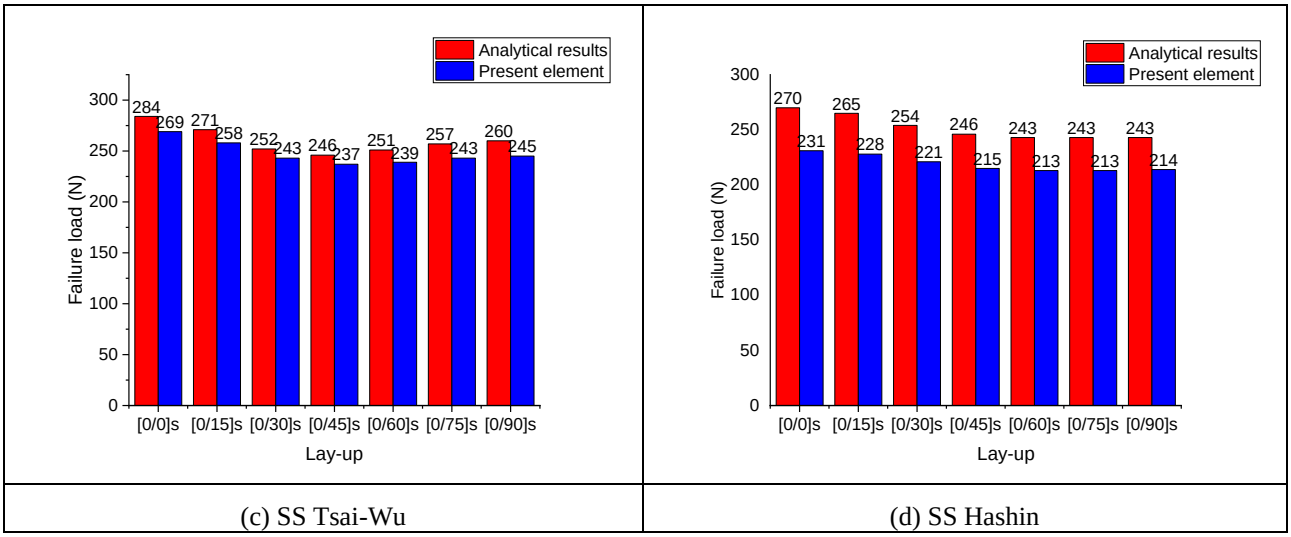
BC	Lay-up	Tsai-Wu criteria		Hashin criteria	
		Analytical results	Present element	Analytical results	Present element
CC	$[90°/0°]_s$	623.482	620.43	581.314	560.25
	$[90°/15°]_s$	532.822	512.07	493.220	472.49
	$[90°/30°]_s$	653.232	611.30	608.010	561.00
	$[90°/45°]_s$	706.818	651.10	660.578	624.96
	$[90°/60°]_s$	754.393	741.30	715.507	702.72
	$[90°/75°]_s$	812.226	813.20	779.074	763.65
	$[90°/90°]_s$	826.519	810.30	793.125	777.36
SS	$[90°/0°]_s$	1314.711	1253.50	1230.280	1145.00
	$[90°/15°]_s$	1501.663	1434.80	1393.435	1299.40
	$[90°/30°]_s$	1545.721	1460.90	1563.488	1478.70
	$[90°/45°]_s$	1577.599	1508.70	1601.870	1533.10
	$[90°/60°]_s$	1620.306	1561.00	1650.878	1591.60
	$[90°/75°]_s$	1661.383	1628.20	1661.383	1595.00
	$[90°/90°]_s$	1706.522	1639.10	1673.060	1605.70



(a) CC Tsai-Wu

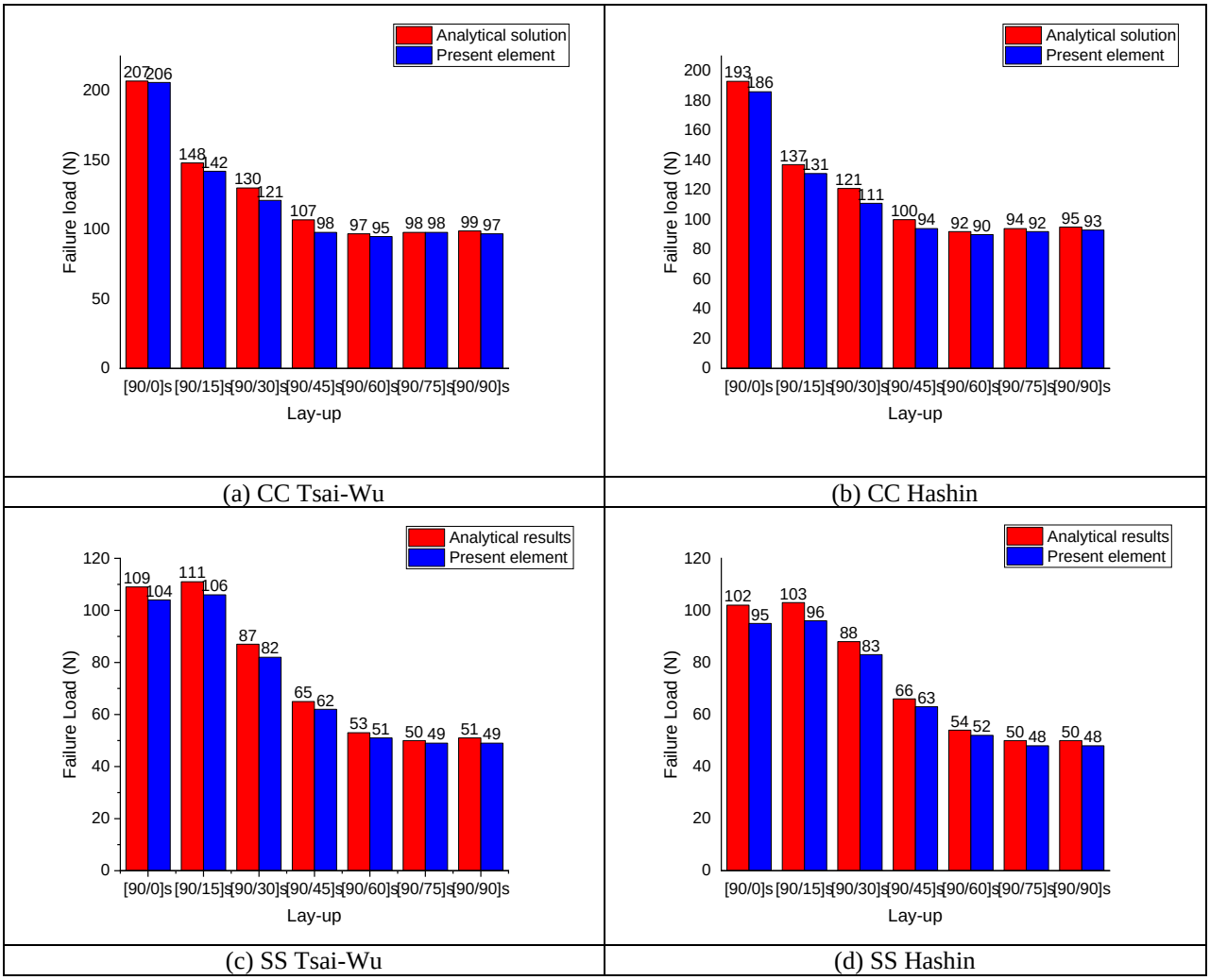


(b) CC Hashin



(c) SS Tsai-Wu (d) SS Hashin

Fig. 4. FPF loads (N) of clamped and simply supported [0°/θ°]s glass/epoxy beams using different failure criterion



(a) CC Tsai-Wu (b) CC Hashin

(c) SS Tsai-Wu (d) SS Hashin

Fig. 5. FPF loads (N) of clamped and simply supported [90°/θ°]s glass/epoxy beams using different failure criterion

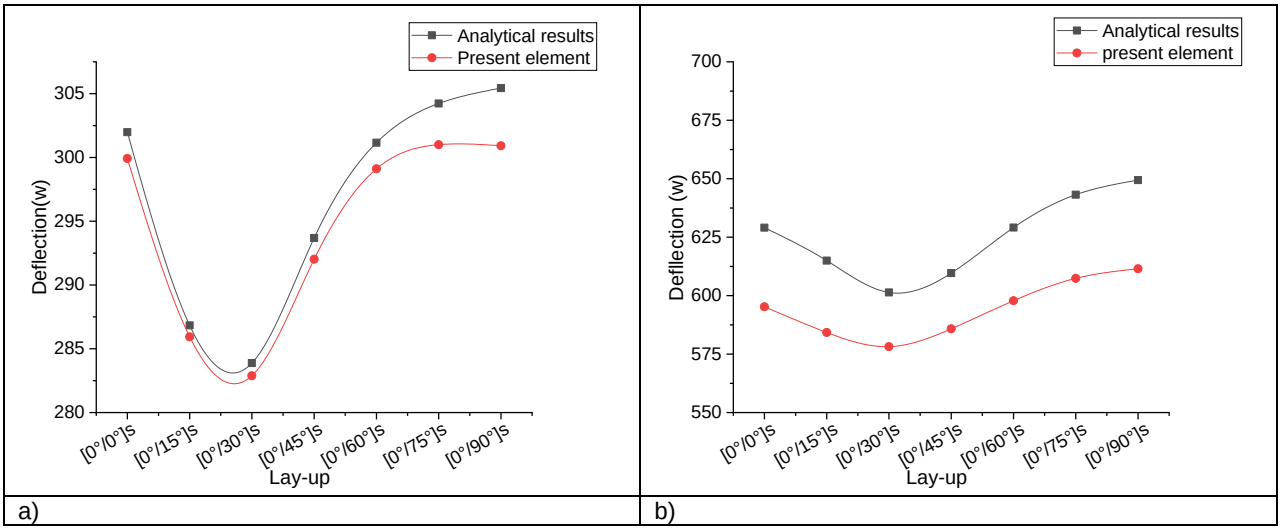


Fig. 6. Deflection of FPF load of (a) clamped and (b) simply supported [0°/θ°]s glass/epoxy beams using Tsai-wu failure criterion

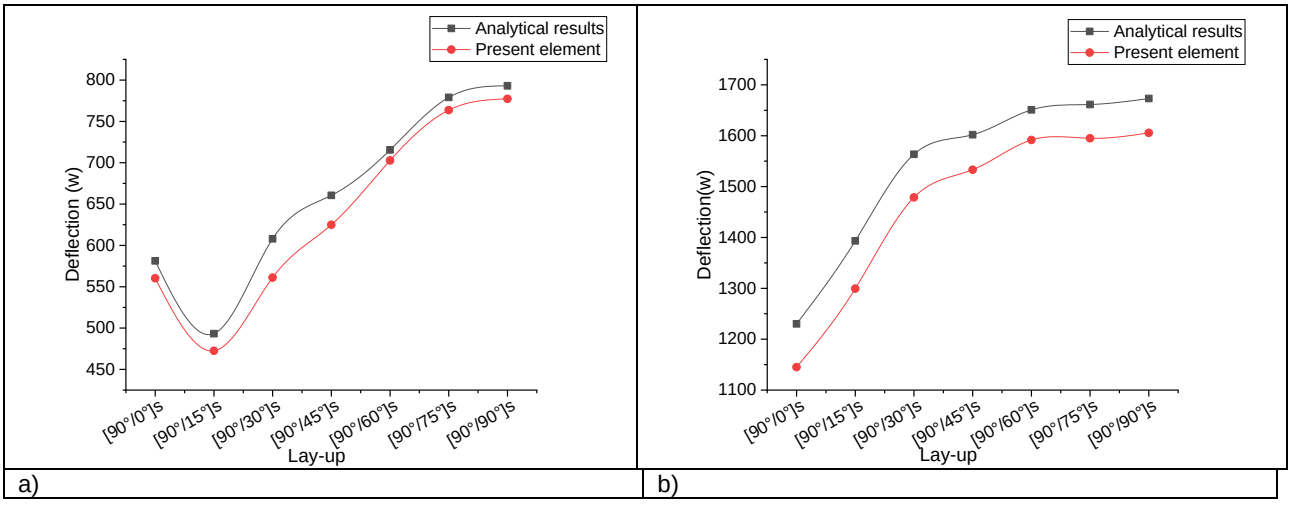


Fig. 7. Deflection (w) of FPF loads (N) of (a) clamped and (b) simply supported [90°/θ°]s glass/epoxy beams using Hachin failure criterion

From Tables 10 and 11, it is observed that the clamped beam with layers [0°/0°]s has the highest FPF load. One can see also from Table 10 that, by increasing the fiber orientation angle, the failure load decreases until it reaches its minimum value for [0°/45°]s beams then it increases to reach a local maximum value for [0°/90°]s. In addition to the previous observations, one can see from Table 11 and Figure 5 that, if the fiber orientation angles are ranging between 0° and 45°, the failure load is completely affected. The augmentation of fiber orientation angle decreases the values of FPF load to reach its minimum value for [90°/60°]s. However, when the angle values are 60°, 75°, and 90°, the strength of the beams is not affected too much and they are quite

close. Thus, whatever the boundary condition is, the increase in the fiber orientation angle reduces the flexural stiffness of the beam and therefore decreases the failure strength.

Table 12 and Figure 6 demonstrates that when increasing the fiber orientation angle, the deflection (w) of failure load decreases until it reaches its minimum value of [0°/30°]s beams, then it increases to reach a local maximum value of [0°/90°]. One can also see that the beam with layers [0°/90°]s has the highest deflection value (w) of the FPF load, in both cases of boundary condition (clamped and simply).

We notice in Table 13 and Figure 7 for a clamped supported beam that the value of deflection decreases with an increase in the fiber orientation until it reaches [0°/15°] and then increases until it reaches its maximum value when the fiber orientation [0°/90°]. In the case of a simply supported beam, the deflection value of FPF increases as the fiber orientation increases until it reaches its maximum value when the fiber orientation is [0°/90°].

In addition to the previous observations, one can see from Tables 11 and 12 and Figures 6 and 7 that the deflection of FPF obtained by the present element is very close to the analytical results because the value of FPF was also close.

Progressive damage analysis: (Failure index)

One of the main purposes of progressive damage analysis of laminated beams is to evaluate the macroscopic damage initiation and propagation using the finite element method. As an example of modeling damage growth, the damage initiation and growth in [0°/90°]s glass/epoxy laminated beams are studied using the present element and Tsai-Wu criteria. The considered beam is clamped from one side and simply supported from the other (CS), and it is subjected to a concentrated load at the mid-span of the beam. As the first step for progressive damage analysis, The initial failure load, commonly known as the first ply failure load (FPF), should be determined as the first step in a progressive damage analysis. Based on the previous examples, the FPF load of this beam is 330N (see Table 9).

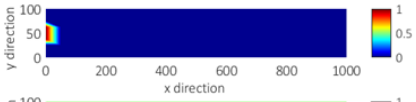
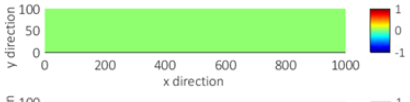
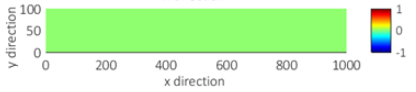
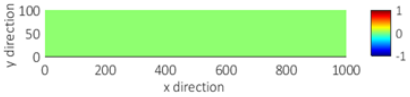
After the first ply failure, it can be assumed that the material properties of the failed elements are not modified, and the laminated beam is reanalyzed at the current load.

The load is applied incrementally in steps (step-by-step), and the damage growth in each surface of the laminated composite beam is determined using this iterative process. The distributions of damage to the laminated beam are shown in Table 14. From the figures, it is observed that:

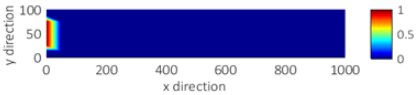
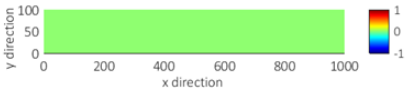
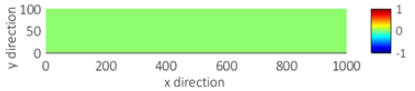
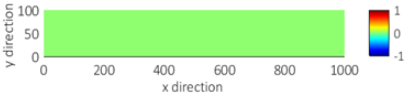
- The damage starts at the clamped side of the beam, where the stresses are significantly higher.
- The damage starts at the top surface of the first ply.
- Since the laminate beam is symmetric, one can suppose that the damage occurs symmetrically along the thickness. However, it is not the case considering this example.
- By increasing the applied load, one can see the damage propagation at the top surface of the first ply. The damage starts from the clamped side, and it propagates.
- When the applied load reaches 340 N, the damage occurs at the bottom surface of the last layer, and then it propagates by increasing the applied load.

Table 14. *The failure strength distribution for beams* $[0/90]_s$ *with (CS) boundary condition with*

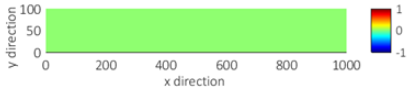
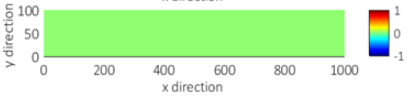
N=330N

Layer	Top surface	Bottom surface
1		
4		

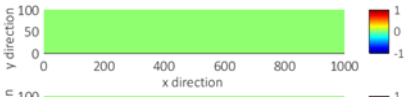
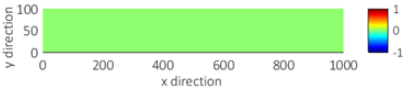
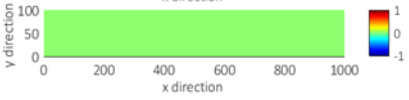
N=340N

Layer	Top surface	Bottom surface
1		
4		

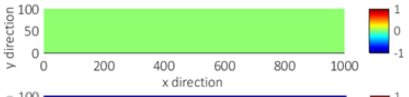
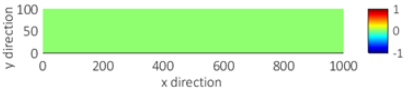
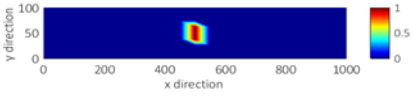
N=360N

Layer	Top surface	Bottom surface
1		
4		

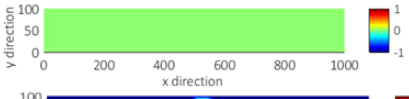
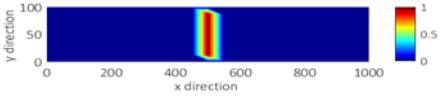
N=380N

Layer	Top surface	Bottom surface
1		
4		

N=400N

Layer	Top surface	Bottom surface
1		
4		

N=420N

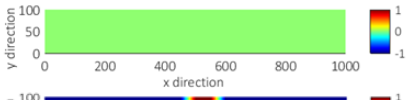
Layer	Top surface	Bottom surface
1		
4		

N=440N

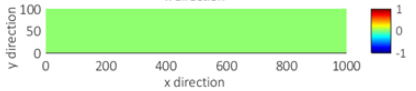
Layer | Top surface | Bottom surface

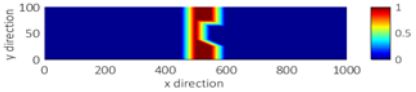
1





4



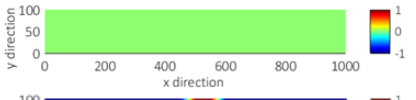


N=460N

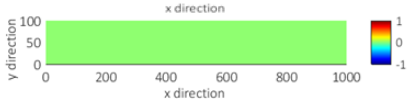
Layer | Top surface | Bottom surface

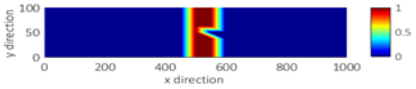
1





4



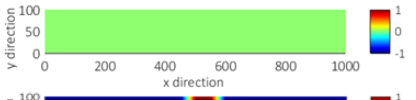


N=480N

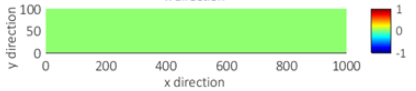
Layer | Top surface | Bottom surface

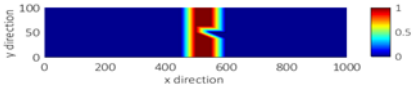
1





4



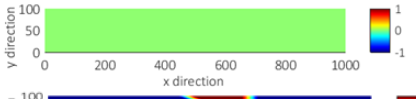


N=500N

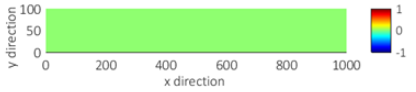
Layer | Top surface | Bottom surface

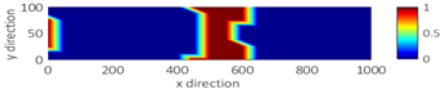
1





4



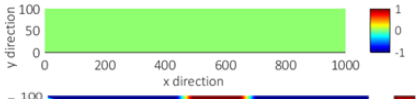


N=520N

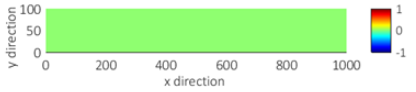
Layer | Top surface | Bottom surface

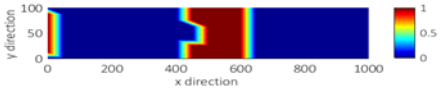
1





4





CONCLUSIONS

This paper studies the first ply failure load (FPF) in ply laminated composite beam subjected to bending loading. Maximum stress criterion, Tsai-Wu, Tsai–Hill and Hashin failure criterion are used in a finite element code, based upon the classical laminate theory, a four-node quadrilateral finite element with six degrees of freedom at each node. Several parameters, such as

fiber orientations, stacking sequences, and boundary conditions, are considered in order to determine and understand their effects on the strength of these laminated plates. The numerical results obtained by the current element compare favorably with those given by the analytical approach. The numerical results are observed to be very close to the analytical results, showing the accuracy of the current element. Some broad conclusions may be drawn from the results presented in the previous section.

- The maximum transverse displacement and FPF loads of glass-epoxy laminated beams were compared using various failure criteria, various schemes of loadings, and different boundary conditions. It can be observed that the BC and loading have a remarkable impact on the FPF loads. The highest value of FPF load, 482.00, is obtained for CC glass/epoxy laminated beams under a concentrated load.
- Two different configurations of stacking sequences, $[0°/\theta°]_s$ and $[90°/\theta°]_s$, are considered to know the effect of fiber orientation on FPF load by using Hashin and Tsai-Wu criterion. The results obtained by these criterions are slightly different. For $[90°/90°]_s$ CC glass/epoxy laminated beams, the failure loads obtained by Hashin and Tsai-Wu criterions are 793.12 and 826.52, respectively.
- Tsai-Wu criteria are used to investigate the initiation and growth of damage in $[0°/90°]_s$ glass-epoxy laminated beams. The considered beam is clamped from one side and simply supported from the other (CS), and it is subjected to a concentrated load at the mid-span of the beam (Progressive damage analysis) we noticed that the damage starts at the top surface and at the clamped side of the beam.

REFERENCES

1. Tsai, S.W., Wu, E.M., A general theory of strength for anisotropic materials. Journal of Composite Materials, 5(1) (1971) 58-80. https://doi.org/10.1177/002199837100500106
2. Hill, R., A theory of the yielding and plastic flow of anisotropic metals. Proceedings of the Royal Society of London. Series A. Mathematical and Physical Sciences, 193(1033) (1948) 281-297. https://doi.org/10.1098/rspa.1948.0045
3. Hoffman, O., The brittle strength of orthotropic materials. Journal of Composite Materials, 1(2) (1967) 200-206. https://doi.org/10.1177/002199836700100210
4. Jones, R.M., Mechanics of composite materials, 2018 CRC Press.
5. Yeh, H.-L., Quadric surfaces criterion for composite materials. Journal of Reinforced Plastics and Composites, 22(6) (2003) 517-532. https://doi.org/10.1106/073168403023274
6. Yeh, H.-L., Yeh, H.-Y., The modified quadric surfaces criterion for composite materials. Journal of Reinforced Plastics and Composites, 21(3) (2002) 279-289. https://doi.org/10.1177/0731684402021003110
7. Hashin, Z., Fatigue failure criteria for unidirectional fiber composites. University of Pennsylvania, Philadelphia. 1981.
8. Norris, C., Strength of orthotropic materials subjected to combined stresses, United States Department Of Agriculture Forest Service. 1962.

9. Hart-Smith, L., Predictions of the original and truncated maximum-strain failure models for certain fibrous composite laminates. Composites Science and Technology, 58(7) (1998) 1151-1178. https://doi.org/10.1016/S0266-3538(97)00192-9
10. Sun, C.-T., Comparative evaluation of failure analysis methods for composite laminates, 1996.
11. Davila, C.G., Camanho, P.P., Rose, C.A., Failure criteria for frp laminates. Journal of Composite Materials, 39(4) (2005) 323-345. https://doi.org/10.1177/0021998305046452
12. Puck, A., Kopp, J., Knops, M., Guidelines for the determination of the parameters in puck's action plane strength criterion. Composites Science and Technology, 62(3) (2002) 371-378. https://doi.org/10.1016/S0266-3538(01)00202-0
13. Catalanotti, G., Camanho, P., Marques, A., Three-dimensional failure criteria for fiber-reinforced laminates. Composite Structures, 95 (2013) 63-79. https://doi.org/10.1016/j.compstruct.2012.07.016
14. Gutkin, R., Pinho, S., Review on failure of laminated composites: experimental perspective and modelling. 2016.
15. Hill, R., The mathematical theory of plasticity. Vol. 11. 1998: Oxford University Press.
16. Berthelot, J.-M., Composite materials: mechanical behavior and structural analysis. Mechanical Engineering Series. 1999: Springer.
17. Azzi, V., Tsai, S.W., Anisotropic strength of composites. Experimental Mechanics, 5(9) (1965) 283-288.
18. Kim, Y., Davalos, J.F., Barbero, E.J., Progressive failure analysis of laminated composite beams. Journal of Composite Materials, 30(5) (1996) 536-560. https://doi.org/10.1177/002199839603000501
19. Lezgy Nazargah, M., Meshkani, Z., An efficient partial mixed finite element model for static and free vibration analyses of fgm plates rested on two-parameter elastic foundations. Structural Engineering And Mechanics, An International Journal, 66(5) (2018.) 665-676.
20. Lezgy Nazargah, M., A high-performance parametrized mixed finite element model for bending and vibration analyses of thick plates. Acta Mechanica, 227(12) (2016) 3429-3450. https://doi.org/10.1007/s00707-016-1676-4
21. Lezgy Nazargah, M., Salahshuran, S., A new mixed-field theory for bending and vibration analysis of multi-layered composite plate. Archives Of Civil And Mechanical Engineering, 18(3) (2018) 818-832. https://doi.org/10.1016/j.acme.2017.12.006
22. Irhirane, E.H., Echaabi, J., Aboussaleh, M., Hattabi, M., Trochu, F., Matrix and fibre stiffness degradation of a quasi-isotrope graphite epoxy laminate under flexural bending test. Journal of Reinforced Plastics and Composites, 28(2) (2009) 201-223. https://doi.org/10.1177/0731684407084213
23. Moncada, A.M., Chattopadhyay, A., Bednarcyk, B.A., Arnold, S.M., Micromechanics-based progressive failure analysis of composite laminates using different constituent failure theories. Journal of Reinforced Plastics and Composites, 31(21) (2012) 1467-1487. https://doi.org/10.1177/0731684412456330
24. Hasan, Z., Muliana, A., Failure and deformation analyses of smart laminated composites. Mechanics of Composite Materials, 48(4) (2012) 391-404. https://doi.org/10.1007/s11029-012-9285-3

25. Daniel, I.M., Constitutive behavior and failure criteria for composites under static and dynamic loading. Meccanica, 50(2) (2015) 429-442. https://doi.org/10.1007/s11012-013-9829-1

26. Lezgy-Nazargah, M., Assessment of refined high-order global–local theory for progressive failure analysis of laminated composite beams. Acta Mechanica, 228(5) (2017) 1923-1940. https://doi.org/10.1007/s00707-017-1807-6

27. Ounis, H., Tati, A., Benchabane, A., Thermal buckling behavior of laminated composite plates: a finite-element study. Frontiers of Mechanical Engineering, 9(1) (2014) 41-49. https://doi.org/10.1007/s11465-014-0284-z

28. Khechai, A., Tati, A., Guettala, A., Finite element analysis of stress concentrations and failure criteria in composite plates with circular holes. Frontiers of Mechanical Engineering, 9(3) (2014) 281-294. https://doi.org/10.1007/s11465-014-0307-9